

Electron-only Reconnection in Kinetic-Alfvén Turbulence

Cristian Vega¹, Vadim Roytershteyn², Gian Luca Delzanno³, and Stanislav Boldyrev^{1,2}

Department of Physics, University of Wisconsin–Madison, Madison, WI 53706, USA; csvega@wisc.edu

Space Science Institute, Boulder, CO 80301, USA

T-5 Applied Mathematics and Plasma Physics Group, Los Alamos National Laboratory, Los Alamos, NM 87545, USA

Received 2019 December 19; revised 2020 February 21; accepted 2020 March 11; published 2020 April 9

Abstract

We study numerically small-scale reconnection events in kinetic, low-frequency, quasi-2D turbulence (termed kinetic-Alfvén turbulence). Using 2D particle-in-cell simulations, we demonstrate that such turbulence generates reconnection structures where the electron dynamics do not couple to the ions, similarly to the electron-only reconnection events recently detected in the Earth's magnetosheath by Phan et al. Electron-only reconnection is thus an inherent property of kinetic-Alfvén turbulence, where the electron current sheets have limited anisotropy and, as a result, their sizes are smaller than the ion inertial scale. The reconnection rate of such electron-only events is found to be close to 0.1.

Unified Astronomy Thesaurus concepts: Magnetic fields (994); Alfven waves (23); Space plasmas (1544)

1. Introduction

Magnetic reconnection has long been considered as one of the fundamental mechanisms of plasma heating and particle acceleration in astrophysical and space plasmas (e.g., Biskamp 2005; Priest & Forbes 2007). Analytical and numerical studies have established that in a collisionless, two-component plasma, where the ions and electrons are not strongly coupled, a reconnection layer generally has at least a two-scale structure: inside an ion-scale current sheet whose thickness is comparable to the ion inertial length d_i , there is a thinner electron-scale current sheet, whose thickness in on the order of the electron inertial length d_e (e.g., Karimabadi et al. 2007; Shay et al. 2007). Magnetic-field lines, frozen into the electrons, reconnect at the electron scale on a short electron timescale, setting up electron outflows along the current sheet. At much larger scales, of the order of d_i and sometimes significantly exceeding it, the electron outflows couple to the ions, leading to the plasma outflow from the reconnection layer on the ion scales.

Recent observations of the Earth's magnetosheath by the NASA Magnetospheric Multiscale mission have, however, drawn attention to reconnection events where only the electron reconnection layers have been detected, without the accompanying ion outflows (Phan et al. 2018; see also previous studies of Yordanova et al. 2016; Vörös et al. 2017; Wilder et al. 2018). Similar electron-only reconnection events were found in the hybrid Vlasov-Maxwell simulations in Califano et al. (2018) when fluctuation energy was injected close to the ion kinetic scale. In these electron-only reconnection events, typical signatures of reconnection where identified, such as the characteristic magnetic and current profiles, the presence of diverging bidirectional electron-Alfvénic jets, but no ion jets were found. An explanation suggested by Phan et al. (2018) pointed out that the ion dynamics was not observed because the overall dimensions of the sheets were smaller than the typical scale (several d_i) required for efficient ion coupling to the electron streams. This suggestion is consistent with the results of previous hybrid simulations (e.g., Mandt et al. 1994) and particle-in-cell (PIC) simulations (e.g., Sharma Pyakurel et al. 2019) that indicate that a length of the reconnection layer of about $5-10d_i$ is needed to observe a "traditional" reconnection site, with efficient coupling of the electron and ion outflows.

Noting that the electron-only events are detected in a turbulent plasma environment, Stawarz et al. (2019) studied the observational properties of corresponding magnetosheath turbulence. They found that these properties are largely consistent with the energy spectra and intermittency observed in other cases of sub-ion-scale plasma turbulence. They also found the instances of energy-spectrum steepening at the scales associated with the electron inertial length ($\lesssim 4d_e$), possibly indicating energy dissipation associated with the electron reconnection events.

These recent observations may suggest that the electron-only reconnection events may, in fact, be a characteristic property of subproton turbulence itself. This question is studied in the present work. A general association between turbulence and magnetic reconnection has long been proposed. More recently, it has received solid backing from kinetic simulations (e.g., Karimabadi et al. 2013) and theoretical analyses in both magnetohydrodynamic and kinetic regimes (Boldyrev & Loureiro 2017. 2019: Loureiro & Boldyrev 2017a, 2017b, 2018, 2020; Mallet et 2017a, 2017b). The latter works in particular suggest that magnetized turbulence may always contain a small-scale subrange where the energy cascade is mediated by the tearing instability.

In order to investigate whether such a subproton-scale energy cascade may indeed be the cause for the electron-only reconnection events, we study the 2D PIC numerical simulations of collisionless subproton-scale turbulence for two regimes. The first regime is characterized by a small electron beta, in particular, $\beta_e \ll \beta_i \lesssim 1$. (For each particle species α the plasma beta is related to the ratio of their gyroscale (ρ_α) to their inertial scale (d_α) , $\beta_\alpha = \rho_\alpha^2/d_\alpha^2$.) Such parameters are common for Earth's magnetosheath and also are expected to be relevant for the vicinity of the solar corona that will soon be studied with the Parker Solar Probe mission. Subproton-scale turbulence in such a regime has been recently studied analytically in Boldyrev & Loureiro (2019), which provides a

⁴ Close to the solar corona, it is expected that $\beta_e \ll \beta_i < 1$ (say, $\beta_e \sim 0.01$, $\beta_i \sim 0.1$). However, at scales smaller than ρ_i , we expect that our analysis will still be applicable.

useful guidance for interpreting our results. We will refer to turbulence regime analyzed here as kinetic-Alfvén, which is implied to mean fully nonlinear plasma turbulence in the phase space region where linear modes are kinetic-Alfvén waves. This region is characterized by high obliquity, $k_{\perp} \gg k_{\parallel}$, and low frequency, $\omega \ll kv_{Ti}$, of the fluctuations (e.g., Mangeney et al. 2006; Alexandrova et al. 2008; Boldyrev et al. 2015; Chen 2016; Chen & Boldyrev 2017). The second studied regime is characterized by a large electron beta, $\beta_e \sim \beta_i \lesssim 1$, typical of larger heliospheric distances. We compare the results obtained in this regime with the results for low electron beta.

We observe that the electron-only reconnection structures are indeed generated by kinetic turbulence, in both considered regimes. The electron reconnection events and the corresponding electron-Alfvén outflows that we find are rather similar to those observationally detected by Phan et al. (2018). Our findings lend support to the idea that such an electron-only regime of magnetic reconnection is an inherent property of turbulence. In order to further support this suggestion, we notice that the analytic studies of tearing-mediated kinetic-Alfvén turbulence (Boldyrev & Loureiro 2019) indicate that subproton-scale turbulence imposes certain limitations on the aspect ratio of the generated electron current sheets. As a result, the current layers with dimensions less than the ion scales, required for the electron-only reconnection, are naturally produced in such a turbulent flow.

2. Simulations

In this work, we identify and characterize reconnection events in subproton-scale plasma turbulence. We analyze the 2D PIC simulations corresponding to the two regimes, $\beta_e = 0.04$, $\beta_i = 0.4$ and $\beta_e = \beta_i = 0.5$. The simulations were conducted using the VPIC code (Bowers et al. 2008). The ratio of the plasma electron frequency to the electron cyclotron frequency was $\omega_{pe}/\Omega_{ce}=2$, and the particle mass ratio was $m_i/m_e = 100$. The simulation plane was perpendicular to the mean magnetic field B_0 oriented in the z direction. The simulation domain was square with sides of length $L_x = L_y = 8\pi d_i = 80\pi d_e \approx 251 d_e$. The low electron beta simulation, corresponding to $\beta_e = 0.04$, $\beta_i = 0.4$, had a resolution of $n_x = n_y = 3456$ cells, 4000 particles per cell per species, and a time step satisfying $\omega_{\rm pe} \, \delta t \approx 0.05$. The numerical setup for these simulations has previously been discussed in more detail in Roytershteyn et al. (2019). The other simulation, corresponding to $\beta_e = \beta_i = 0.5$, had a resolution of $n_x = n_y = 1024$ cells, 10,000 particles per cell per species, and a time step $\omega_{\rm pe} \delta t \approx 0.17$.

In both regimes, decaying turbulence was seeded by imposing randomly phased perturbations of the type

$$\delta \mathbf{B} = \sum_{k} \delta \mathbf{B}_{k} \cos(\mathbf{k} \cdot \mathbf{x} + \chi_{k}), \tag{1}$$

$$\delta \mathbf{V} = \sum_{k} \delta \mathbf{V}_{k} \cos(\mathbf{k} \cdot \mathbf{x} + \phi_{k}), \tag{2}$$

with the wavenumbers $\mathbf{k} = \{2\pi m/L_x, 2\pi n/L_y\}$, with m = -2,...,2 and n = 0,...,2. The initial energy of the magnetic and kinetic fluctuations was about $\mathcal{E} \approx 0.01 B_0^2$. The turbulence then evolved for several eddy turnover times (the eddy turnover time being approximately $30\Omega_{\rm ci}^{-1}$) before our analysis was performed.

In order to find the *X*-points, we note that in a 2D plane, magnetic field can be computed from a potential function:

$$\mathbf{B}_{\perp} = \nabla \times (\psi \hat{\mathbf{z}}) = \frac{\partial \psi}{\partial y} \hat{\mathbf{x}} - \frac{\partial \psi}{\partial x} \hat{\mathbf{y}}.$$
 (3)

Since $\mathbf{B}_{\!\perp} \cdot \nabla \psi = 0$, the in-plane magnetic field is tangent to the contour lines of ψ , so this function must have a saddle point wherever there is reconnection. To find ψ , we start from the Ampère–Maxwell law. In the nonrelativistic regime, the displacement current can be dropped, obtaining

$$\nabla \times \mathbf{B}_{\perp} = \mathbf{J}_{z}. \tag{4}$$

Using (3) we get the following Poisson equation:

$$\nabla^2 \psi = -J_7. \tag{5}$$

The equation above was solved using a 2D Poisson solver based on Matlab's fast Fourier transform.

In order to find the saddle points of the magnetic potential, the first and second derivatives of ψ were computed numerically. Since the numerical gradient of the potential is never exactly zero, we identified as saddle points those points where the determinant of the Hessian matrix was negative and the first derivatives were less than 1% of the standard deviation of the derivatives themselves over the whole domain. A similar approach was used in several prior studies (e.g., Haggerty et al. 2017, and references therein).

The data used were time averaged over the time interval corresponding to several consecutive time steps (approximately spanning one-fifth of the electron gyration period), which considerably reduced noise in the out-of-plane electric field. Additional Fourier and Gaussian space filtering (Haggerty et al. 2017) had a very weak effect on the results, likely because the statistical noise was already low thanks to the large number of particles and time averages. Consequently, only the time average was used to obtain the results presented here.

3. Results

Figure 1 shows the saddle points found at some typical snapshots in $\beta_e = 0.04$ and $\beta_e = 0.5$ simulations. A reconnection site was marked in each case with an X, with the red line corresponding to the direction of the outflow and the green line to the inflow. Figure 2 shows the corresponding reconnecting component of the magnetic field (B_1) , the electron inflow and outflow velocities (U_{e2} and U_{e1}), the ion inflow and outflow velocities (U_{i2} and U_{i1}), the electron density (n_e), and the outof-plane current profile (J_z) along the inflow and outflow directions. The velocities were normalized to the electron-Alfvén velocity computed with the reconnecting magnetic field. The latter was estimated as half the jump of the magnetic field across the electron inflow layer. The magnetic field was normalized by the guide field B_0 , which is perpendicular to the simulation plane. Remarkably, we find that in these reconnection sites, the ions do not couple to the electron inflow and outflow, which is similar to the observational results by Phan et al. (2018).

In order to understand why the ions do not couple to the electron motion, it is instructive to analyze the sizes of the out-of-plane current sheets characterized by the current density J_z . In the case $\beta_e = 0.04$ (left panel in Figure 2), the thickness of the current sheet is about $a \sim d_e$, while its width is about $w \sim 4d_e$. In the case of $\beta_e = 0.5$ (right panel in Figure 2), the

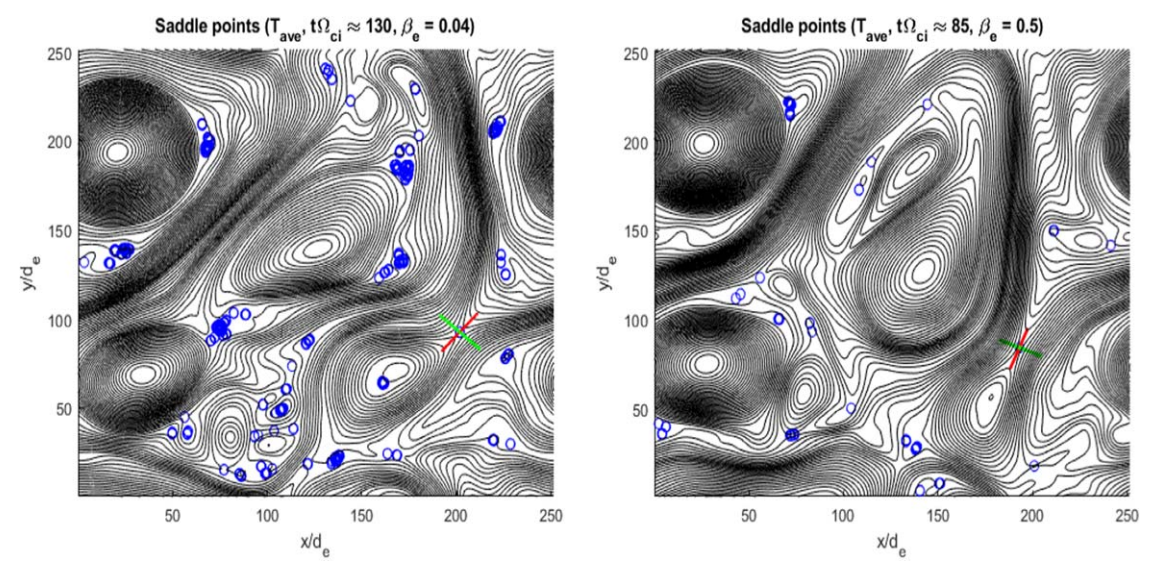


Figure 1. Contour lines of the magnetic potential ψ . The left panel corresponds to kinetic-Alfvén turbulence with $\beta_e = 0.04$, the right one to $\beta_e = 0.5$. Saddle points of ψ are denoted by blue circles. The electron-only reconnection events are discovered in both cases; the specific regions analyzed in detail below are marked by the green–red crosses. The directions of the red and green lines mark the (orthogonal) directions of the Hessian eigenvectors at the corresponding saddle points.

current sheet dimensions are slightly larger. In both cases, however, the sizes of the current sheets and of the electron outflow regions are significantly smaller than the typical scale ($\sim 10 \ d_i$), which has been proposed to be necessary for the electron outflows to couple to the ions (e.g., Mandt et al. 1994; Phan et al. 2018; Sharma Pyakurel et al. 2019).

In addition to looking at the aforementioned current sheets we developed an algorithm to automatically identify and measure the dimensions of all out-of-plane current sheets potentially corresponding to reconnection events. To construct the current sheets we first identify all the points of the grid where the current is above a certain threshold (chosen to be 3 times the rms current). Then we find the local maxima of the current among those points. This is done by looking at the current on a square window of side 2n + 1 centered on the point of interest (we used n = 3). If the current at that point is the maximum in that window, it is regarded as a local maximum. Once the local maxima have been found they are ordered from highest to lowest. Starting on the point with the highest current, its four closest neighbors are checked, and if the current on any of them is found to be above a certain threshold (chosen to be some fraction of the peak corresponding to that current sheet) that point is taken to be part of the current sheet. The neighbors of the new points are then checked and so on until the current on all the points surrounding the current sheet is below the threshold (while for all the points in the current sheet it is above). When this process is completed for one maximum, the program moves on to the next local maximum. If this one belonged to any of the current sheets already found the program skips to the next maximum. The current sheets that overlap with the saddle points found previously are said to correspond to reconnection events. This algorithm, which was implemented in Matlab, is based on the algorithm previously discussed in Zhdankin et al. (2013).

The width w of a current sheet is taken to be the largest distance between any two points belonging to the sheet. The thickness a is measured as the size of the current sheet in the direction of the most rapid descent from the peak. Figure 3 shows the current sheets found in both the low and high electron beta simulations, at a particular time, with the

threshold that defines the current sheets set to three-fourths of the sheet's peak. The red crosses highlight the current peaks corresponding to current sheets that overlap with saddle points (potential reconnection sites). Interestingly, in the high electron beta case the algorithm was able to identify only one current sheet containing a saddle point, which is the current sheet corresponding to the example discussed above. The current sheet width determined by our algorithm was $14.6 d_e$ and the thickness was $1.23 d_e$. In the low electron beta case, five such sheets were found by our algorithm, including the example that we discussed previously in Figure 2. The obtained current-sheet widths ranged from 3.2 to $18.1 d_e$ (the average was $7.9 d_e$). The thicknesses ranged from 0.36 to $0.95 d_e$ (the average was $0.57 d_e$).

We checked that out of the five reconnecting current sheets found by the algorithm in the low electron beta case, the profiles corresponding to the *X*-points with coordinates $(x/d_e, y/d_e) = (104.4, 37.38)$ and $(x/d_e, y/d_e) = (143.9, 221.7)$ have a structure qualitatively similar to the electron-only reconnection event shown in Figure 2. For the remaining two points, with coordinates $(x/d_e, y/d_e) = (94.68, 34.18)$ and $(x/d_e, y/d_e) = (168.4, 23.71)$, it is harder to clearly identify an electron inflow and outflow due to the strongly asymmetric structures of the current sheets, as can be seen in Figure 3.

The small lengths of the detected current sheets are likely related to the fact that these current sheets are self-consistently generated by kinetic-scale turbulence. Note that Boldyrev & Loureiro (2019) proposed that the kinetic-Alfvén turbulent cascade in low electron beta, $\beta_e \ll \beta_i \lesssim 1$, 3D turbulence generates sheared magnetic structures (turbulent eddies) that become tearing-unstable already for a relatively limited field-perpendicular aspect ratio. It may, therefore, be reasonable to expect that the dimensions of the resulting electron

⁵ In order to understand how generic such a situation is, we applied the algorithm to several other randomly selected snapshots in both the low and high electron beta simulations, finding from five to eight reconnection sites per snapshot in the former case and from one to three in the latter. This suggests that these electron-only reconnection events are easier to generate in the low electron beta environment.

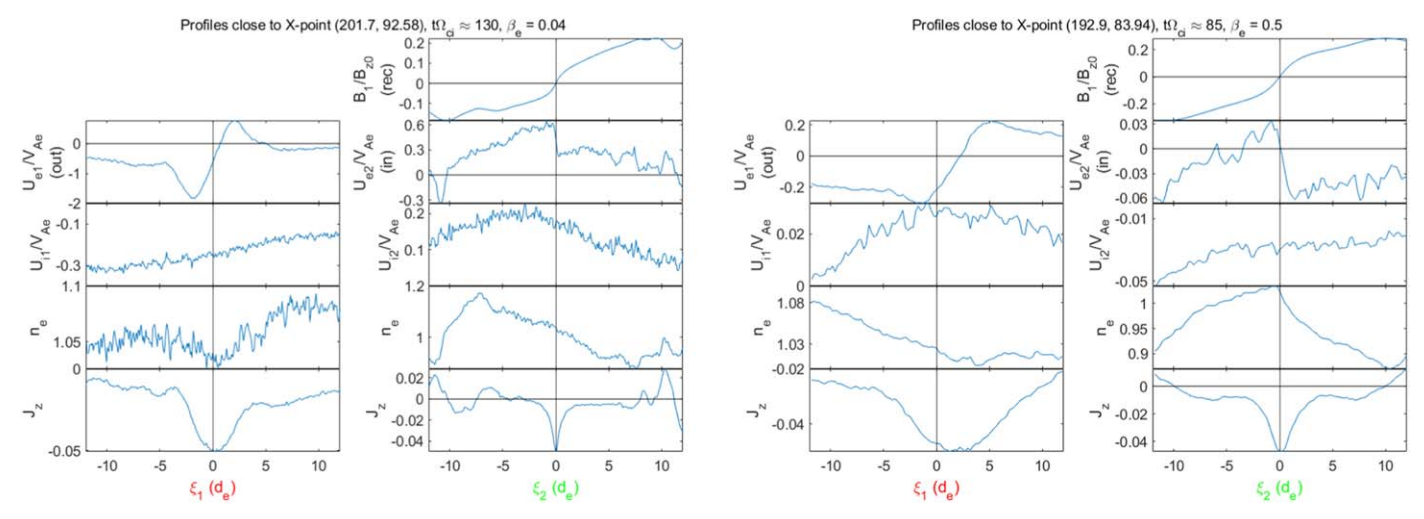


Figure 2. Profiles close to the X-points marked in Figure 1. Direction ξ_1 corresponds to the Hessian eigenvector associated with the outflow direction, while ξ_2 is close to the inflow direction. The X-point found by the Matlab algorithm is located at $\xi_1 = \xi_2 = 0$. In the $\beta_e = 0.5$ example, the peak of the J_z profile and the zero of the outflow velocity deviate from the position of the X-point, which is expected since the reconnection layer is not symmetric (e.g., Cassak & Shay 2007; Doss et al. 2015). In both cases, there also appears to be a large-scale plasma flow at the X-point, which formally leads to nonzero mean electron and ion flows in the reconnection layer.

reconnection layers also remain limited and, in particular, smaller than the ion scales.⁶ Further, our simulations suggest that similar conclusion holds for the regimes with $\beta_i \sim \beta_e \sim 1$. We see that the observed aspect ratio of the current sheets in the case $\beta_e \sim \beta_i$ is qualitatively similar to that of the low electron beta case (even though the number of detected electron-only reconnecting sites in the large-beta case is smaller). Analytically, the similar behavior in the low and high electron beta regimes can be understood in the following way. In Passot et al. (2017) it is shown that the finite Larmour radius corrections to the nonlinear equations governing the dynamics of the low electron beta plasma are on the order of $k_{\perp}^2 \rho_e^2$, which needs to be added to terms proportional to $k_{\perp}^2 d_e^2$. When $\rho_e \sim d_e$, the finite Larmour radius corrections are on the order of the inertial terms, so while they can renormalize the numerical coefficients, they are not expected to qualitatively change the dynamics.

Finally, we measured the reconnection rate of the electrononly reconnection sites in both the low and high electron beta simulations. In order to estimate the reconnection rate, several traditional methods can be used. First, one can define the reconnection rate by using the magnetic and electric fields on the scale of the electron layer, which is by definition a local reconnection rate (e.g., Cassak et al. 2017). We found, however, that in the case of low electron beta, the electron inflow velocity $U_{e,2}$ does not agree with the formally calculated E×B velocity, E_z/B_2 . The latter, measured at distance $\pm a$ from the midplane of the reconnection layer, produces a several times larger value than the electron inflow velocity directly measured from Figure 2. This may be related to the presence of strong gradients of the electric field, gradients of pressure, and electron inertial effects inside the structure. A second way of measuring the reconnection rate is by finding the ratio of the electron inflow velocity to the electron outflow velocity for each reconnecting current sheet. This method was also found to be unreliable, giving in some cases reconnection rates above unity. This may be due to the difficulties in identifying the right points to measure the inflow and outflow velocities in the case of asymmetric current sheets.

On the other hand, from the relation $U_{\rm inflow}/U_{\rm outflow} \sim a/w$, which is valid in a steady state, one can define the reconnection rate as the aspect ratio of a current sheet, a/w, which can be reliably measured by our algorithm. We, therefore, use the aspect ratio of the reconnecting current sheets as a proxy for their reconnection rates. The average reconnection rate obtained in this way in the low electron beta case was 0.093, while in the high electron beta case it was 0.084. The aspect ratio a/w was also calculated for other values of the threshold used to define the current sheets, producing qualitatively similar results. Rather interestingly, the results are close to 0.1, which demonstrates that the previously established result on collisionless magnetic reconnection (e.g., Birn et al. 2001; Comisso & Bhattacharjee 2016; Cassak et al. 2017) also applies to the novel electron-only reconnection regime.

4. Conclusions

In this work, we addressed the possible origin of the electron-only reconnection events recently discovered in the Earth's magnetosheath observations (Phan et al. 2018). In order to effectively decouple from the ions, the electron reconnection layers and the corresponding electron outflow jets should be confined to sufficiently small regions, smaller than about $5-10 d_i$, as estimated in numerical simulations (e.g., Mandt et al. 1994; Sharma Pyakurel et al. 2019). Our results support the conjecture that such electron-only reconnection events may be a direct consequence of subproton turbulence in general, and the kinetic-Alfvén turbulence in particular. We analyzed the 2D PIC numerical simulations of kinetic-Alfvén turbulence in two regimes, corresponding to low electron beta, $\beta_e \ll \beta_i \sim 1$, and high electron beta, $\beta_e \sim \beta_i \sim 1$. We have observed that the electron-only reconnection events are naturally generated in both cases (although, possibly, more efficiently in the low-beta case), with the corresponding electron and ion profiles quite similar to those observed in the Earth's magnetosheath. The

⁶ We point out that the theory of Boldyrev & Loureiro (2019) deals with the tearing instability, which is an initial stage of reconnection, while here we discuss fully nonlinear current sheets appearing after an *X*-point collapse.

We also note that a similar analysis can be conducted in the regime $\beta_e \sim \beta_i \ll 1$; see Mallet (2019).

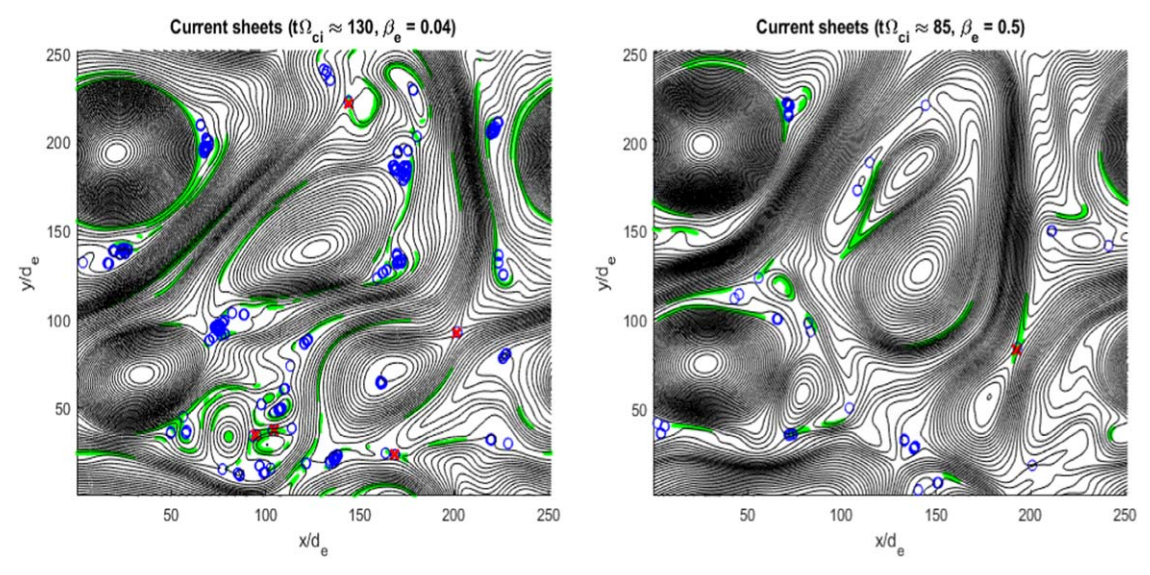


Figure 3. Current sheets found (in green). The red crosses are the current peaks of those sheets containing saddle points (blue circles).

width of the electron current layers is on average $8d_e$ ($\lesssim d_i$) in the low-beta regime and seems to be larger in the high-beta regime, but still significantly below the scale of about 5–10 d_i required for the electron—ion coupling.

A theory of tearing-mediated kinetic-Alfvén turbulence recently proposed in Boldyrev & Loureiro (2019) predicts that such turbulence should generate tearing-unstable magnetic profiles whose scales are smaller than the ion inertial scale. Therefore, we expect that electron-only reconnection should be a general feature of such regimes. Note that the theory of Boldyrev & Loureiro (2019) was developed for the simplified case of small electron beta, $\beta_e \ll \beta_i \sim 1$. Our study found that electron-only reconnection is also characteristic of large electron beta, $\beta_e \sim \beta_i \sim 1$. Moreover, we observed that the reconnection rates in both cases are comparable to the wellknown "standard" value of 0.1. Our analysis of low electron beta kinetic-Alfvén turbulence will be especially relevant, among other astrophysical and space environments, for the vicinity of the solar corona that will soon be studied with the new NASA Parker Solar Probe mission.

This research was partially supported by the Los Alamos National Laboratory (LANL) through its Center for Space and Earth Science (CSES). CSES is funded by LANL's Laboratory Directed Research and Development (LDRD) program under project number 20180475DR. The work of S.B. was partly supported by the NSF under grant No. NSF PHY-1707272, by NASA under grant No. NASA 80NSSC18K0646, and by DOE grant No. DE-SC0018266. V.R. was partly supported by NASA grant NNX15AR16G. Computational resources were provided by the NASA High-End Computing Program through the NASA Advanced Supercomputing Division at Ames Research Center. PIC simulations were conducted as a part of the Blue Waters sustained-petascale computing project, which is supported by the National Science Foundation (awards OCI-0725070 and ACI-1238993) and the state of Illinois. Blue Waters is a joint effort of the University of Illinois at Urbana-Champaign and its National Center for Supercomputing Applications. Blue Waters allocation was provided by the National Science Foundation through PRAC award 1614664.

ORCID iDs

Vadim Roytershteyn https://orcid.org/0000-0003-1745-7587

Stanislav Boldyrev https://orcid.org/0000-0001-6252-5169

References

Alexandrova, O., Lacombe, C., & Mangeney, A. 2008, AnGeo, 26, 3585
Birn, J., Drake, J. F., Shay, M. A., et al. 2001, JGR, 106, 3715
Biskamp, D. 2005, Magnetic Reconnection in Plasmas (Cambridge: Cambridge Univ. Press)
Boldyrev, S., Chen, C. H. K., Xia, Q., & Zhdankin, V. 2015, ApJ, 806, 238

Boldyrev, S., Chen, C. H. K., Xia, Q., & Zhdankin, V. 2015, ApJ, Boldyrev, S., & Loureiro, N. F. 2017, ApJ, 844, 125

Boldyrev, S., & Loureiro, N. F. 2019, PhRvR, 1, 012006

Bowers, K. J., Albright, B. J., Yin, L., Bergen, B., & Kwan, T. J. T. 2008, PhPl, 15, 055703

Califano, F., Cerri, S. S., Faganello, M., Laveder, D., & Kunz, M. W. 2018, arXiv:1810.03957

Cassak, P. A., Liu, Y. H., & Shay, M. A. 2017, JPIPh, 83, 715830501

Cassak, P. A., & Shay, M. A. 2007, PhPl, 14, 102114

Chen, C. H. K. 2016, JPIPh, 82, 535820602

Chen, C. H. K., & Boldyrev, S. 2017, ApJ, 842, 122 Comisso, L., & Bhattacharjee, A. 2016, JPIPh, 82, 595820601

Doss, C. E., Komar, C. M., Cassak, P. A., et al. 2015, JGRA, 120, 7748

Haggerty, C. C., Parashar, T. N., Matthaeus, W. H., et al. 2017, PhPl, 24, 102308

Karimabadi, H., Daughton, W., & Scudder, J. 2007, GeoRL, 34, L13104

Karimabadi, H., Roytershteyn, V., Wan, M., et al. 2013, PhPl, 20, 012303

Loureiro, N. F., & Boldyrev, S. 2017a, PhRvL, 118, 245101

Loureiro, N. F., & Boldyrev, S. 2017b, ApJ, 850, 182

Loureiro, N. F., & Boldyrev, S. 2018, ApJL, 866, L14

Loureiro, N. F., & Boldyrev, S. 2020, ApJ, 890, 55

Mallet, A. 2019, arXiv:1912.02286

Mallet, A., Schekochihin, A. A., & Chandran, B. D. G. 2017a, MNRAS, 468, 4862

Mallet, A., Schekochihin, A. A., & Chandran, B. D. G. 2017b, JPIPh, 83, 905830609

Mandt, M. E., Denton, R. E., & Drake, J. F. 1994, GeoRL, 21, 73

Mangeney, A., Lacombe, C., Maksimovic, M., et al. 2006, AnGeo, 24, 3507 Passot, T., Sulem, P. L., & Tassi, E. 2017, JPIPh, 83, 715830402

Phan, T. D., Eastwood, J. P., Shay, M. A., et al. 2018, Natur, 557, 202

Priest, E., & Forbes, T. 2007, Magnetic Reconnection (Cambridge: Cambridge Univ. Press), 2007

Roytershteyn, V., Boldyrev, S., Delzanno, G. L., et al. 2019, ApJ, 870, 103
Sharma Pyakurel, P., Shay, M. A., Phan, T. D., et al. 2019, PhPl, 26, 082307
Shay, M. A., Drake, J. F., & Swisdak, M. 2007, PhRvL, 99, 155002
Stawarz, J. E., Eastwood, J. P., Phan, T. D., et al. 2019, ApJL, 877, L37
Vörös, Z., Yordanova, E., Varsani, A., et al. 2017, JGRA, 122, 11442
Wilder, F. D., Ergun, R. E., Burch, J. L., et al. 2018, JGRA, 123, 6533

Yordanova, E., Vörös, Z., Varsani, A., et al. 2016, GeoRL, 43, 5969

Zhdankin, V., Uzdensky, D. A., Perez, J. C., & Boldyrev, S. 2013, ApJ, 771, 124